

Supporting Information

Further Exploration on the Physicochemical Nature of μ_2 -Bridge-Relevant Deprotonations via the Elucidation of Four Kinds of Alditol Complexes

Yi Wu,^[a, b, c] Linchen Xie,^[d] Ye Jiang,^[b] Anqi He,^[b] Da Li,*^[c] Limin Yang,*^[a]

Yizhuang Xu,*^[b] Kexin Liu,^[a] Yukihiro Ozaki,^[b,e] Isao Noda^[b,f]

- [a] State Key Laboratory of Nuclear Physics and Technology, Institute of Heavy Ion Physics, School of Physics, Peking University, Beijing 100871, China
- [b] Beijing National Laboratory for Molecular Sciences, State Key Laboratory for Rare Earth Materials Chemistry and Applications, College of Chemistry and Molecular Engineering, Peking University, Beijing 100871, China
- [c] School of Biology and Medicine, Beijing City University, Beijing 100094, China
- [d] School of Metallurgical and Ecological Engineering, University of Science and Technology Beijing, Beijing 100083, China
- [e] School of Biological and Environmental Sciences, Kwansei Gakuin University, Sanda, Hyogo 669-1330, Japan
- [f] Department of Materials Science and Engineering, University of Delaware, Newark, DE 19716, United States

* The corresponding authors. Telephone: 86-10-62757951, E-mail: xyz@pku.edu.cn, yanglm@pku.edu.cn, lida.lnzyydx@163.com

List of Supporting Information

- Part 1 Description of the structure of LuG
- Part 2 Description of the structure of ScI
- Part 3 Description of the structure of MnG
- Part 4 Description of the structure of SrIN
- Part 5 The pKa's of *myo*-inositol according to the prediction by the chemicalize program
- Part 6 Mass spectra of LuG, ScI, MnG, and SrIN
- Part 7 The variation of pH values of aqueous solutions upon the addition of alditols
- Part 8 The bond lengths and torsion angles in ScI and ErI
- Part 9 The structural characteristics of galactitol and its metal complexes
- Part 10 Quantum chemistry calculation results for galactitol

Part 1 Description of the structure of LuG

The ORTEP diagram of LuG is shown in Figure S1-1. The packing diagram is shown in Figure S1-2. Selected bond lengths are listed in Table S1-1. Selected bond angles are listed in Table S1-2. Hydrogen bonds of the complex are listed in Table S1-3. Torsion angles of the complex are listed in Table S1-4.

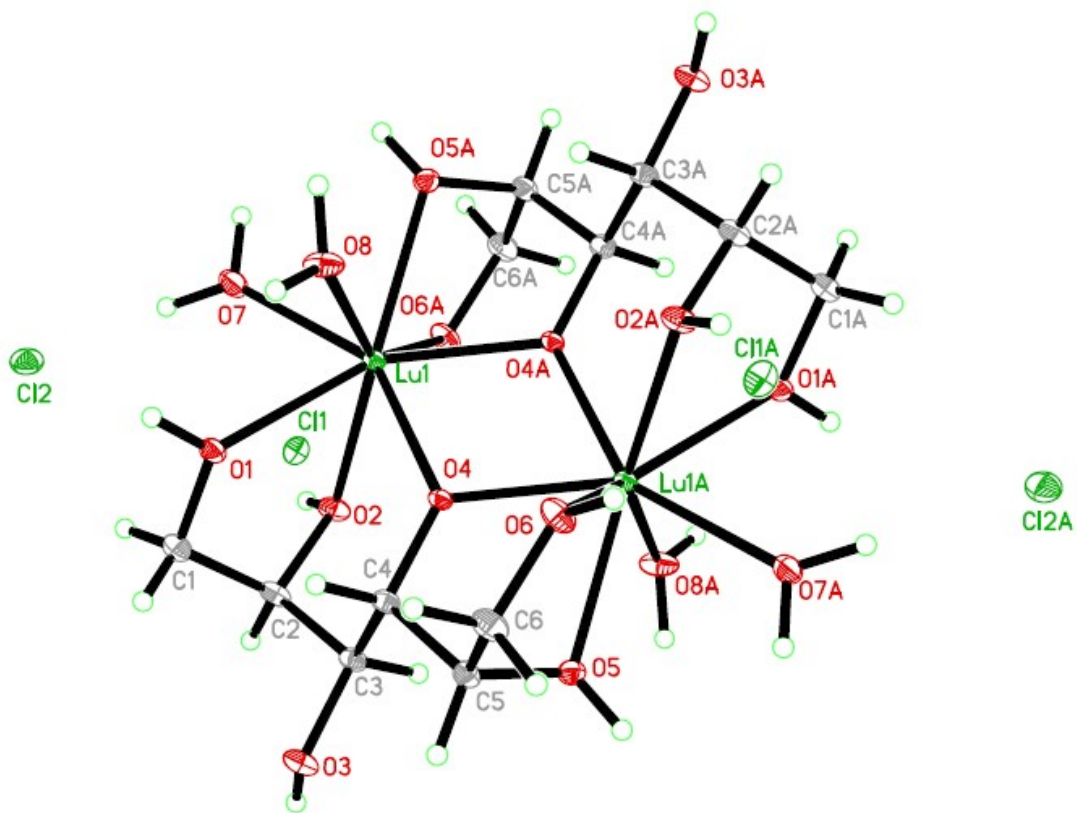


Figure S1-1. ORTEP diagram of LuG

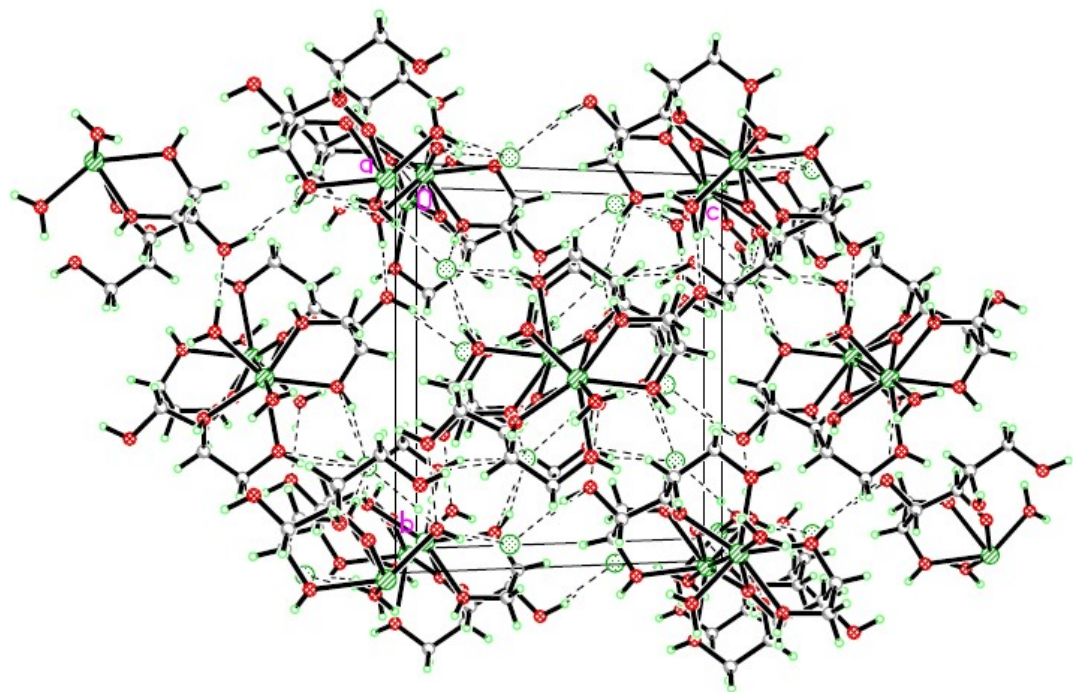


Figure S1-2. Packing diagram of LuG along the *b*-axis

Table S1-1. Bond Lengths for LuG.

	Length/Å		Length/Å
Lu1–O4	2.207(3)	O4–C4	1.424(4)
Lu1–O4 ¹	2.223(3)	O4–Lu1 ¹	2.223(3)
Lu1–O8	2.239(3)	O5–C5	1.443(5)
Lu1–O7	2.324(3)	O5–Lu1 ¹	2.360(3)
Lu1–O2	2.327(3)	O6–C6	1.442(5)
Lu1–O5 ¹	2.360(3)	O6–Lu1 ¹	2.388(3)
Lu1–O1	2.365(3)	C1–C2	1.495(6)
Lu1–O6 ¹	2.387(3)	C2–C3	1.531(6)
Lu1–Lu1 ¹	3.6411(4)	C3–C4	1.530(5)
O1–C1	1.443(5)	C4–C5	1.519(6)
O2–C2	1.452(4)	C5–C6	1.524(5)
O3–C3	1.426(4)		

¹-X, 1-Y, 1-Z**Table S1-2.** Bond Angles for LuG.

	Angle/°		Angle/°
O7–Lu1–O5 ¹	75.20(10)	C6–O6–Lu1 ¹	116.8(2)
O2–Lu1–O5 ¹	139.18(9)	O1–C1–C2	106.7(3)
O4–Lu1–O1	76.36(10)	O2–C2–C1	109.0(3)
O4 ¹ –Lu1–O1	144.39(10)	O2–C2–C3	108.6(3)
O8–Lu1–O1	74.93(10)	C1–C2–C3	115.9(3)
O7–Lu1–O1	73.95(11)	O3–C3–C4	107.7(3)
O2–Lu1–O1	67.58(10)	O3–C3–C2	108.0(3)
O5 ¹ –Lu1–O1	135.86(10)	C4–C3–C2	113.3(3)
O4–Lu1–O6 ¹	117.00(11)	O4–C4–C5	108.8(3)
O4 ¹ –Lu1–O6 ¹	73.97(10)	O4–C4–C3	108.6(3)
O8–Lu1–O6 ¹	142.66(10)	C5–C4–C3	112.7(3)
O7–Lu1–O6 ¹	78.85(11)	O5–C5–C4	104.8(3)
O2–Lu1–O6 ¹	72.57(9)	O5–C5–C6	108.9(3)
O5 ¹ –Lu1–O6 ¹	68.76(10)	C4–C5–C6	113.5(3)
O1–Lu1–O6 ¹	132.97(10)	O6–C6–C5	108.4(3)
O4–Lu1–Lu1 ¹	34.86(7)	O4 ¹ –Lu1–Lu1 ¹	34.58(6)
O4–Lu1–O4 ¹	69.44(10)	O8–Lu1–Lu1 ¹	93.93(9)
O4–Lu1–O8	90.86(10)	O7–Lu1–Lu1 ¹	174.83(8)
O4 ¹ –Lu1–O8	95.58(11)	O2–Lu1–Lu1 ¹	94.54(8)
O4–Lu1–O7	149.15(10)	O5 ¹ –Lu1–Lu1 ¹	101.97(7)
O4 ¹ –Lu1–O7	141.17(10)	O1–Lu1–Lu1 ¹	110.70(7)
O8–Lu1–O7	89.46(12)	O6 ¹ –Lu1–Lu1 ¹	96.12(8)
O4–Lu1–O2	75.91(10)	C1–O1–Lu1	120.9(2)
O4 ¹ –Lu1–O2	111.80(10)	C2–O2–Lu1	114.9(2)

O8–Lu1–O2	142.17(10)	C4–O4–Lu1	129.0(2)
O7–Lu1–O2	85.13(11)	C4–O4–Lu1 ¹	119.9(2)
O4–Lu1–O5 ¹	134.17(10)	Lu1–O4–Lu1 ¹	110.56(10)
O4 ¹ –Lu1–O5 ¹	69.39(10)	C5–O5–Lu1 ¹	106.2(2)
O8–Lu1–O5 ¹	74.00(10)		

¹-X, 1-Y, 1-Z

Table S1-3. Hydrogen Bonds for LuG.

D–H… A	d(D-H)/Å	d(H…A)/Å	d(D…A)/Å	D-H-A/°
O1–H1…Cl11	0.922(19)	2.15(2)	3.055(3)	168(4)
O2–H2…Cl11	0.939(19)	2.11(2)	3.003(3)	159(4)
O3–H3…Cl22	0.941(19)	2.18(2)	3.103(3)	167(4)
O5–H5…Cl13	0.932(19)	2.15(2)	3.061(3)	166(4)
O6–H6…Cl14	0.945(19)	2.30(3)	3.183(3)	156(4)
O7–H7A…Cl2	0.945(19)	2.15(2)	3.088(3)	173(4)
O7–H7B…Cl15	0.925(18)	2.265(18)	3.184(3)	173(4)
O8–H8A…O36	0.927(18)	1.78(2)	2.655(4)	157(4)
O8–H8B…Cl27	0.934(18)	2.16(2)	3.074(3)	166(3)

¹1-X, -1/2+Y, 3/2-Z; ²1-X, 1-Y, 2-Z; ³-X, -1/2+Y, 3/2-Z; ⁴-X, 1-Y, 1-Z; ⁵+X, 3/2-Y, -1/2+Z; ⁶+X, 1/2-Y, -1/2+Z; ⁷1-X, 1-Y, 1-Z

Table S1-4. Torsion Angles for LuG.

	Angle/°		Angle/°
Lu1–O1–C1–C2	23.6(4)	O3–C3–C4–O4	178.8(3)
Lu1–O2–C2–C1	50.6(4)	C2–C3–C4–O4	-61.8(4)
Lu1–O2–C2–C3	-76.4(3)	O3–C3–C4–C5	58.3(4)
O1–C1–C2–O2	-45.6(4)	C2–C3–C4–C5	177.6(3)
O1–C1–C2–C3	77.1(4)	Lu1 ¹ –O5–C5–C4	59.7(3)
O2–C2–C3–O3	-165.7(3)	Lu1 ¹ –O5–C5–C6	-62.0(3)
C1–C2–C3–O3	71.4(4)	O4–C4–C5–O5	-49.4(4)
O2–C2–C3–C4	75.1(4)	C3–C4–C5–O5	71.1(4)
C1–C2–C3–C4	-47.8(4)	O4–C4–C5–C6	69.3(4)
Lu1–O4–C4–C5	-174.5(2)	C3–C4–C5–C6	-170.3(3)
Lu1 ¹ –O4–C4–C5	14.7(4)	Lu1 ¹ –O6–C6–C5	-9.7(4)
Lu1–O4–C4–C3	62.5(4)	O5–C5–C6–O6	47.3(4)
Lu1 ¹ –O4–C4–C3	-108.2(3)	C4–C5–C6–O6	-68.9(4)

¹-X, 1-Y, 1-Z

Part 2 Description of the structure of ScI

The ORTEP diagram of ScI is shown in Figure S2-1. The packing diagram is shown in Figure S2-2. Selected bond lengths are listed in Table S2-1. Selected bond angles are listed in Table S2-2. Hydrogen bonds of the complex are listed in Table S2-3. Torsion angles of the complex are listed in Table S2-4.

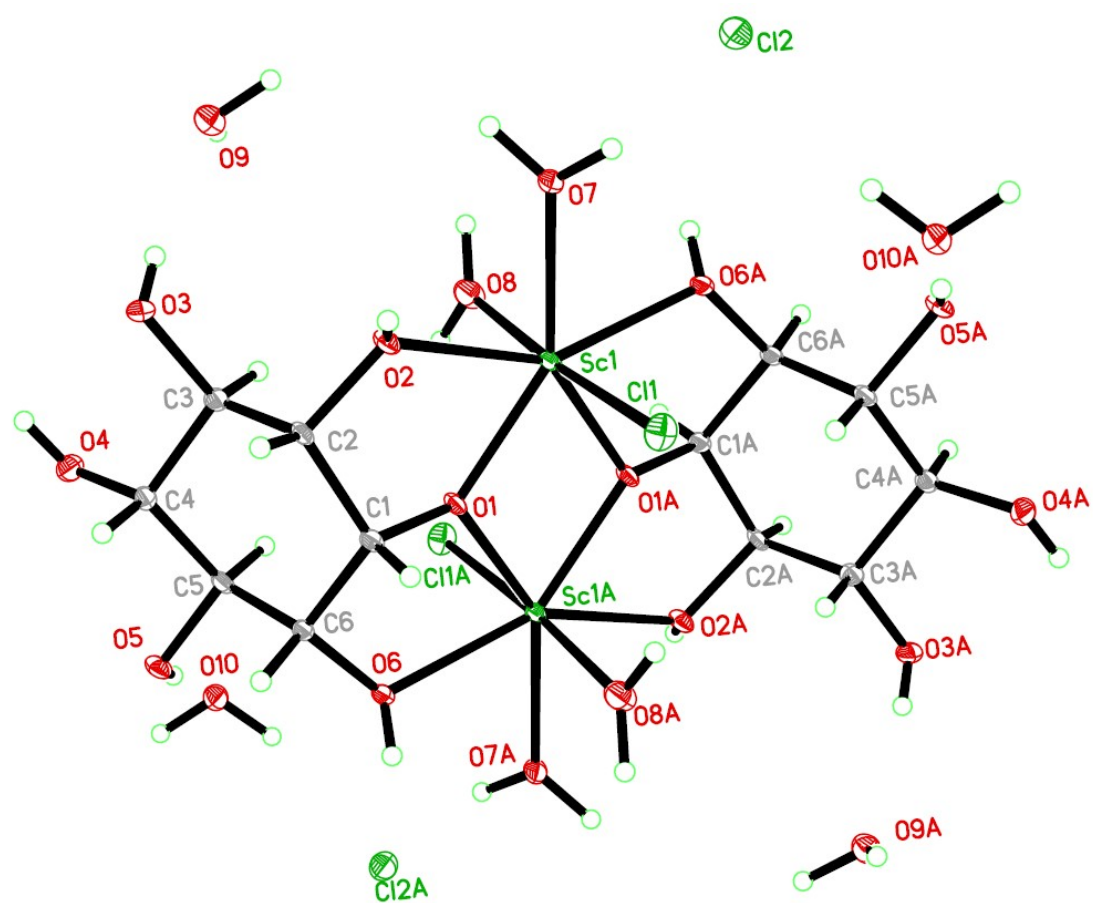


Figure S2-1. The ORTEP diagram of ScI

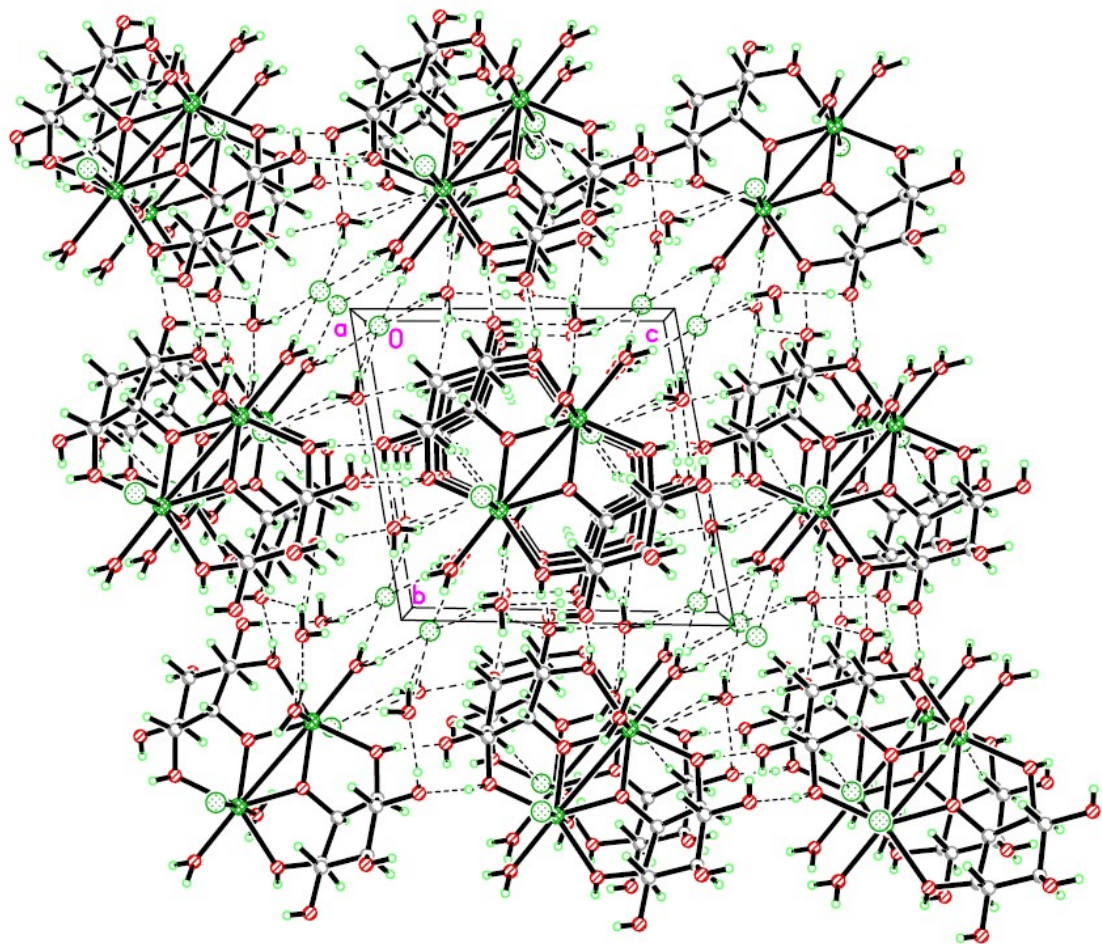


Figure S2-2. The Packing diagram of ScI along the *a*-axis

Table S2-1. Bond Lengths for ScI.

	Length/ \AA		Length/ \AA
Sc1–O1	2.0686(14)	O3–C3	1.436(2)
Sc1–O1 ¹	2.0894(13)	O4–C4	1.414(3)
Sc1–O8	2.1631(16)	O5–C5	1.432(2)
Sc1–O7	2.1915(15)	O6–C6	1.445(2)
Sc1–O6 ¹	2.2410(15)	O6–Sc1 ¹	2.2410(15)
Sc1–O2	2.2628(15)	C1–C6	1.527(3)
Sc1–Cl1	2.4679(7)	C1–C2	1.530(3)
Sc1–Sc1 ¹	3.4311(8)	C2–C3	1.519(3)
O1–C1	1.416(2)	C3–C4	1.517(3)
O1–Sc1 ¹	2.0894(13)	C4–C5	1.518(3)
O2–C2	1.444(2)	C5–C6	1.509(3)

¹1-X, 1-Y, 1-Z

Table S2-2. Bond Angles for ScI.

	Angle/ [°]		Angle/ [°]
O1–Sc1–O1 ¹	68.79(6)	O2–Sc1–Sc1 ¹	105.65(4)
O1–Sc1–O8	89.66(6)	C11–Sc1–Sc1 ¹	93.10(2)
O1 ¹ –Sc1–O8	90.97(6)	C1–O1–Sc1	121.63(11)
O1–Sc1–O7	145.08(6)	C1–O1–Sc1 ¹	121.78(11)
O1 ¹ –Sc1–O7	145.12(6)	Sc1–O1–Sc1 ¹	111.21(6)
O8–Sc1–O7	83.28(6)	C2–O2–Sc1	118.21(11)
O1–Sc1–O6 ¹	139.68(5)	C6–O6–Sc1 ¹	118.06(12)
O1 ¹ –Sc1–O6 ¹	71.28(5)	O1–C1–C6	107.01(15)
O8–Sc1–O6 ¹	85.65(6)	O1–C1–C2	107.59(15)
O7–Sc1–O6 ¹	73.99(6)	C6–C1–C2	114.40(17)
O1–Sc1–O2	71.08(5)	O2–C2–C3	109.30(16)
O1 ¹ –Sc1–O2	139.80(6)	O2–C2–C1	105.47(15)
O8–Sc1–O2	91.05(6)	C3–C2–C1	113.89(16)
O7–Sc1–O2	74.89(6)	O3–C3–C4	108.51(16)
O6 ¹ –Sc1–O2	148.87(5)	O3–C3–C2	109.33(16)
O1–Sc1–Cl1	94.51(4)	C4–C3–C2	111.19(17)
O1 ¹ –Sc1–Cl1	90.63(4)	O4–C4–C3	112.44(16)
O8–Sc1–Cl1	175.83(5)	O4–C4–C5	107.12(16)
O7–Sc1–Cl1	93.21(5)	C3–C4–C5	107.95(16)
O6 ¹ –Sc1–Cl1	91.22(5)	O5–C5–C6	110.11(16)
O2–Sc1–Cl1	90.21(4)	O5–C5–C4	108.96(16)
O1–Sc1–Sc1 ¹	34.59(4)	C6–C5–C4	109.96(16)
O1 ¹ –Sc1–Sc1 ¹	34.20(4)	O6–C6–C5	108.58(16)
O8–Sc1–Sc1 ¹	90.39(5)	O6–C6–C1	105.84(15)
O7–Sc1–Sc1 ¹	173.67(5)	C5–C6–C1	114.14(16)
O6 ¹ –Sc1–Sc1 ¹	105.32(4)		

¹1-X, 1-Y, 1-Z

Table S2-3. Hydrogen Bonds for ScI.

D–H… A	d(D–H)/Å	d(H…A)/Å	d(D…A)/Å	D–H–A/°
O2–H2…O3 ¹	0.79(3)	1.84(3)	2.618(2)	172(3)
O3–H3…O9	0.72(3)	1.97(3)	2.687(2)	173(3)
O4–H4…O9 ²	0.84(3)	1.93(3)	2.760(2)	169(3)
O5–H5…O10	0.75(3)	1.98(3)	2.724(2)	177(3)
O6–H6…O5 ³	0.82(3)	1.78(3)	2.586(2)	164(3)
O7–H7A…Cl2	0.930(16)	2.147(17)	3.0613(17)	168(2)
O7–H7B…Cl2 ⁴	0.957(15)	2.203(17)	3.1356(16)	165(2)
O8–H8A…O10 ⁵	0.895(16)	1.862(18)	2.733(2)	164(2)
O8–H8B…Cl1 ⁶	0.893(16)	2.94(3)	3.3680(18)	110.9(19)
O8–H8B…Cl1 ⁷	0.893(16)	2.809(18)	3.5930(18)	147(2)
O9–H9A…Cl1 ⁶	0.907(15)	2.42(2)	3.1927(17)	143(2)
O9–H9B…Cl2 ⁴	0.926(16)	2.207(16)	3.1070(18)	164(2)
O10–H10A…Cl2 ⁷	0.917(15)	2.285(18)	3.1767(17)	164(2)
O10–H10B…O4 ⁸	0.935(16)	1.990(19)	2.879(2)	158(2)
O10–H10B…O5 ⁸	0.935(16)	2.32(2)	2.955(2)	125(2)

¹1-X, 1-Y, 2-Z; ²2-X, 1-Y, 2-Z; ³1-X, 2-Y, 1-Z; ⁴1-X, -Y, 2-Z; ⁵2-X, 1-Y, 1-Z; ⁶1+X, +Y, +Z; ⁷1-X, 1-Y, 1-Z; ⁸2-X, 2-Y, 1-Z

Table S2-4. Torsion Angles for ScI.

Angle/°		Angle/°	
Sc1–O1–C1–C6	167.09(12)	O3–C3–C4–C5	176.92(16)
Sc1 ¹ –O1–C1–C6	-41.08(19)	C2–C3–C4–C5	-62.8(2)
Sc1–O1–C1–C2	43.7(2)	O4–C4–C5–O5	-53.8(2)
Sc1 ¹ –O1–C1–C2	-164.45(12)	C3–C4–C5–O5	-175.14(16)
Sc1–O2–C2–C3	-97.88(15)	O4–C4–C5–C6	-174.59(16)
Sc1–O2–C2–C1	24.94(18)	C3–C4–C5–C6	64.1(2)
O1–C1–C2–O2	-39.9(2)	Sc1 ¹ –O6–C6–C5	94.04(16)
C6–C1–C2–O2	-158.61(15)	Sc1 ¹ –O6–C6–C1	-28.91(19)
O1–C1–C2–C3	80.0(2)	O5–C5–C6–O6	68.5(2)
C6–C1–C2–C3	-38.8(2)	C4–C5–C6–O6	-171.47(16)
O2–C2–C3–O3	-72.13(19)	O5–C5–C6–C1	-173.75(15)
C1–C2–C3–O3	170.21(16)	C4–C5–C6–C1	-53.7(2)
O2–C2–C3–C4	168.08(15)	O1–C1–C6–O6	41.03(19)
C1–C2–C3–C4	50.4(2)	C2–C1–C6–O6	160.09(16)
O3–C3–C4–O4	59.0(2)	O1–C1–C6–C5	-78.32(19)
C2–C3–C4–O4	179.25(15)	C2–C1–C6–C5	40.7(2)

¹1-X, 1-Y, 1-Z

Part 3 Description of the structure of MnG

The ORTEP diagram of MnG without H atoms is presented in Figure S3-1. The crystallographic data and structural refinement of MnG are listed in Table 1. The ORTEP diagram of MnG where H atoms are included is shown in Figure S3-2. Each structural unit of MnG contains two manganese (II) ions, one galactitol molecule, two H_2O , and four Cl^- . Hence, the empirical formula of the complex is $[\text{Mn}_2(\text{C}_6\text{H}_{14}\text{O}_6)(\text{H}_2\text{O})_2\text{Cl}_4]$, and the molar ratio between Mn^{2+} and galactitol is 2:1. A hydrogen-bonding network is formed among Cl^- and OH groups from galactitol and water molecules. The packing diagram is shown in Figure S3-3. Selected bond lengths are listed in Table S3-1. Selected bond angles are listed in Table S3-2. The hydrogen bonds of the complex are listed in Table S3-3. Torsion angles of the complex are listed in Table S3-4. In the complex, Mn^{2+} is coordinated by two oxygen atoms from a galactitol molecule, an oxygen atom from a water molecule, and three chloride ions. Among the three coordinating Cl^- , two Cl^- take part in the coordination as bridges. Hence, the coordination number of the manganese ion is six. Each galactitol molecule coordinates with two Mn^{2+} . In other words, O2, and O3 of the galactitol molecule coordinate to an Mn^{2+} (Mn1), while O2B and O3B coordinate to another Mn^{2+} (Mn1B) (Figure S3-1). The oxygen atoms from two terminal OH groups of the galactitol do not coordinate with Mn^{2+} , but form hydrogen bonds with O2 atoms from other galactitol molecules. In MnG, no OH group is involved in the formation of any μ_2 -bridge.

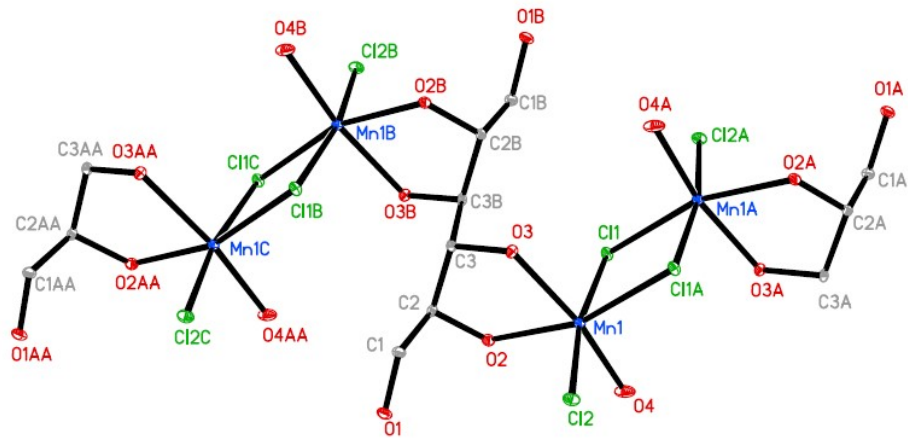


Figure S3-1. The ORTEP diagram of MnG without H atoms

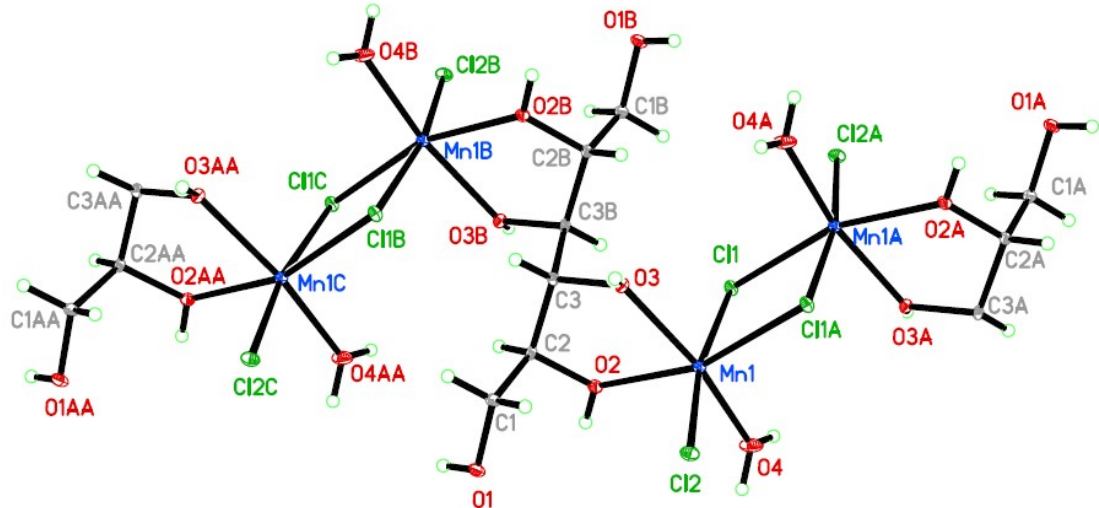


Figure S3-2. The ORTEP diagram of MnG

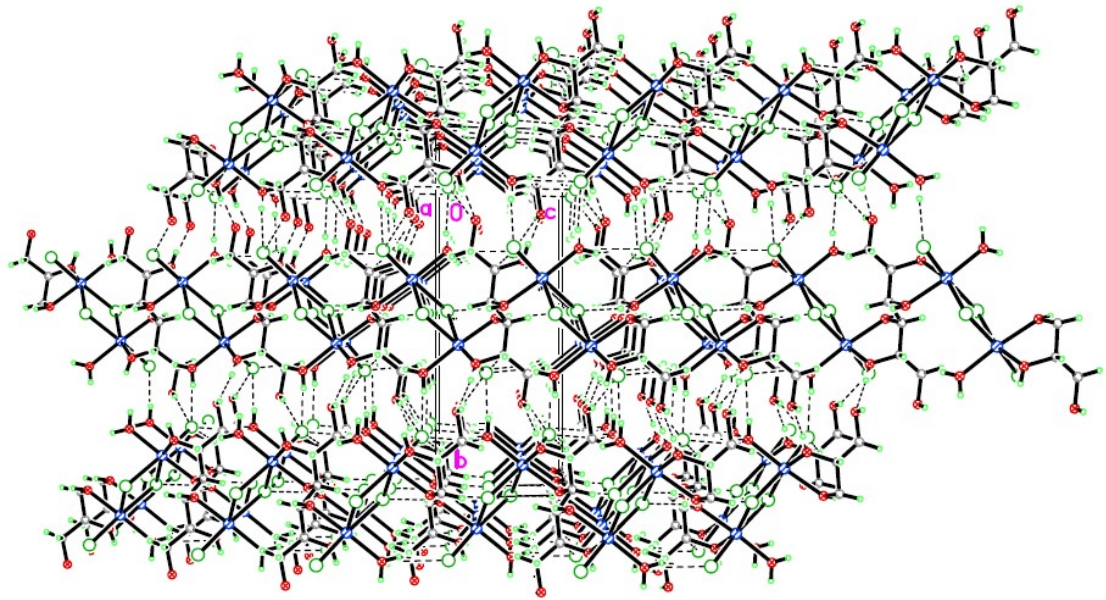


Figure S3-3. The Packing diagram of MnG along the α -axis

Table S3-1. Bond Lengths for MnG.

	Length/ \AA		Length/ \AA
Mn1–Cl1	2.5849(7)	O1–C1	1.436(3)
Mn1–Cl1 ¹	2.5093(6)	O3–C3	1.444(3)
Mn1–Cl2	2.5012(7)	O2–C2	1.445(3)
Mn1–O3	2.1989(16)	C1–C2	1.518(3)
Mn1–O2	2.1821(17)	C3–C3 ²	1.528(5)
Mn1–O4	2.1202(17)	C3–C2	1.531(3)
Cl1–Mn1 ¹	2.5093(6)		

¹-X, 1-Y, -Z; ²1-X, 1-Y, 1-Z

Table S3-2. Bond Angles for MnG.

	Angle/ $^\circ$		Angle/ $^\circ$
Cl1 ¹ –Mn1–Cl1	84.49(2)	O4–Mn1–O3	165.99(7)
Cl2–Mn1–Cl1 ¹	87.62(2)	O4–Mn1–O2	94.40(7)
Cl2–Mn1–Cl1	169.94(2)	Mn1 ¹ –Cl1–Mn1	95.51(2)
O3–Mn1–Cl1 ¹	90.86(4)	C3–O3–Mn1	118.18(13)
O3–Mn1–Cl1	92.69(5)	C2–O2–Mn1	120.13(13)
O3–Mn1–Cl2	93.66(5)	O1–C1–C2	110.8(2)
O2–Mn1–Cl1	90.46(5)	O3–C3–C3 ²	107.1(2)
O2–Mn1–Cl1 ¹	162.14(5)	O3–C3–C2	108.73(18)
O2–Mn1–Cl2	98.90(5)	C3 ² –C3–C2	113.0(2)
O2–Mn1–O1	72.23(6)	O2–C2–C1	110.80(19)
O4–Mn1–Cl1	83.00(5)	O2–C2–C3	106.47(18)
O4–Mn1–Cl1 ¹	101.94(6)	C1–C2–C3	112.4(2)
O4–Mn1–Cl2	92.56(5)		

¹-X, 1-Y, -Z; ²1-X, 1-Y, 1-Z

Table S3-3. Hydrogen Bonds for MnG.

D-H… A	d(D-H)/Å	d(H…A)/Å	d(D…A)/Å	D-H-A/°
O1–H1… Cl2 ¹	0.820	2.645	3.374	148.86
O3–H3… Cl1 ²	0.846	2.254	3.077	164.32
O2–H2… O3 ³	0.845	1.864	2.693	166.39
O4– H4A… Cl2 ⁴	0.852	2.354	3.171	160.70
O4– H4B… Cl2 ³	0.844	2.187	3.023	170.71

¹ X+1, -Y+3/2, Z+1/2; ² X, Y, Z+1; ³ X, -Y+3/2, Z-1/2; ⁴ X, Y, Z-1

Table S3-4. Torsion Angles for MnG.

	Angle/°		Angle/°
Mn1–O3–C3–C3 ¹	-89.0(2)	O3–Mn1–Cl1–Mn1 ²	90.60(4)
Mn1–O3–C3–C2	33.5(2)	O3–Mn1–O2–C2	-12.90(15)
Mn1–O2–C2–C1	-89.4(2)	O3–C3–C2–O2	-40.1(2)
Mn1–O2–C2–C3	33.1(2)	O3–C3–C2–C1	81.4(2)
Cl1 ² –Mn1–Cl1–Mn1 ²	0.0	O2–Mn1–Cl1–Mn1 ²	162.84(5)
Cl1 ² –Mn1–O3–C3	161.44(14)	O2–Mn1–O3–C3	-12.72(14)
Cl1–Mn1–O3–C3	76.91(14)	O4–Mn1–Cl1–Mn1 ²	-102.78(6)
Cl1 ² –Mn1–O2–C2	-32.3(3)	O4–Mn1–O3–C3	5.3(4)
Cl1–Mn1–O2–C2	-105.58(15)	O4–Mn1–O2–C2	171.41(16)
Cl2–Mn1–Cl1–Mn1 ²	-38.51(14)	C3 ¹ –C3–C2–O2	78.7(3)
Cl2–Mn1–O3–C3	-110.89(14)	C3 ¹ –C3–C2–C1	-159.8(2)
Cl2–Mn1–O2–C2	78.11(15)	O1–C1–C2–C3	-177.37(18)
O1–C1–C2–O2	-58.4(2)		

¹1-X, 1-Y, 1-Z; ²-X, 1-Y, -Z

Part 4 Description of the structure of SrIN

The ORTEP diagram of SrIN without H atoms is shown in Figure S4-1. The ORTEP diagram of SrIN with H atoms is shown in Figure S4-2. The crystallographic data and structural refinement of SrIN are listed in Table 1. The packing diagram is shown in Figure S4-3. Selected bond lengths are listed in Table S4-1. Selected bond angles are listed in Table S4-2. Hydrogen bonds of the complex are listed in Table S4-3. Torsion angles of the complex are listed in Table S4-4.

Each structural unit of SrIN contains two strontium(II) ions, two *myo*-inositol molecules, two H₂O, and four NO₃⁻. Thus, the empirical formula of SrIN is [Sr₂(C₆H₁₂O₆)₂(H₂O)₂(NO₃)₄], and the molar ratio between Sr²⁺ and *myo*-inositol is 1:1. A hydrogen-bonding network is formed among nitrate ions and OH groups from *myo*-inositol and water. Each Sr²⁺ is coordinated by two bidentate nitrate ions, one H₂O, and four oxygen atoms from two *myo*-inositol molecules. Hence, the coordination number of Sr²⁺ is nine. A *myo*-inositol molecule provides two oxygen atoms (O1 and O6) to coordinate with one Sr²⁺, and two oxygen atoms (O4 and O5) to coordinate with another Sr²⁺. In SrIN, no OH group is involved in the formation of any μ₂-bridge.

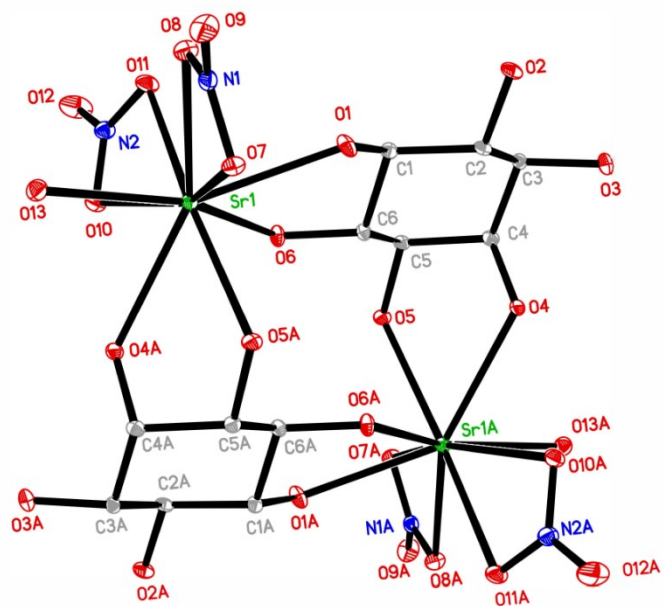


Figure S4-1. The ORTEP diagram of SrIN without H atoms

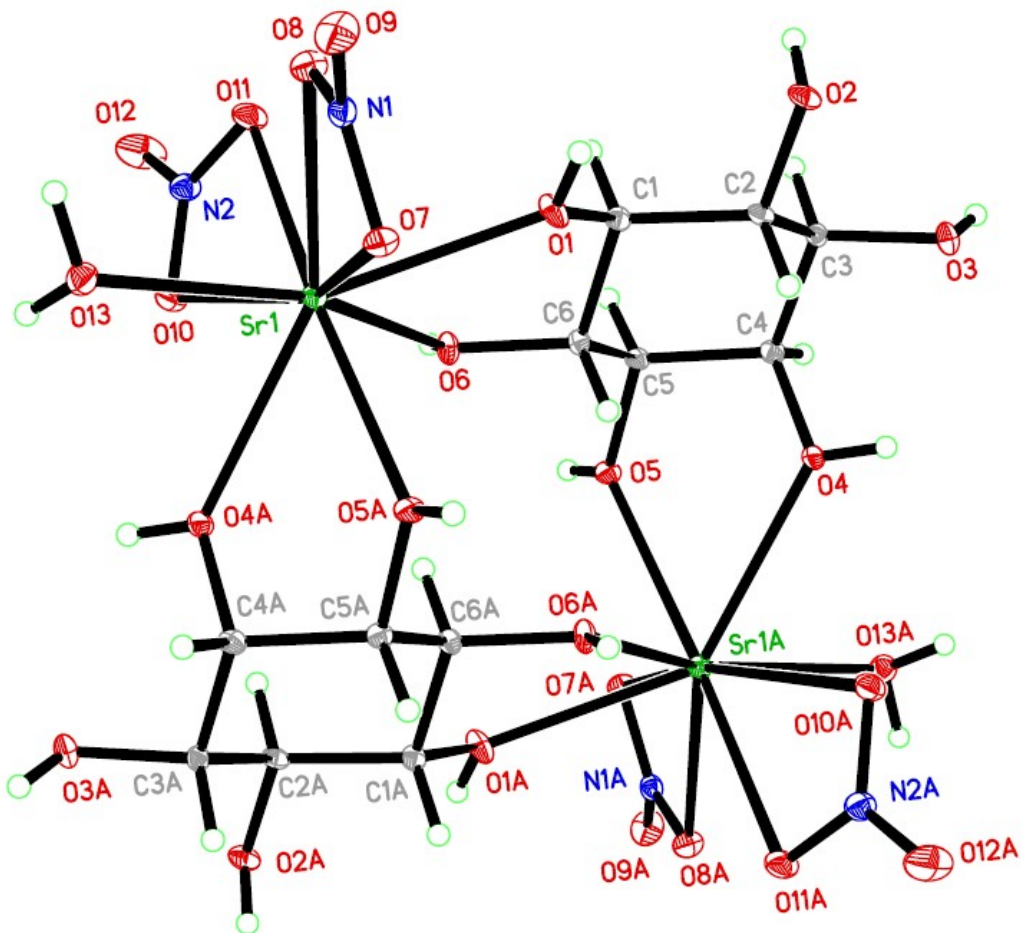


Figure S4-2. The ORTEP diagram of SrIN with H atoms

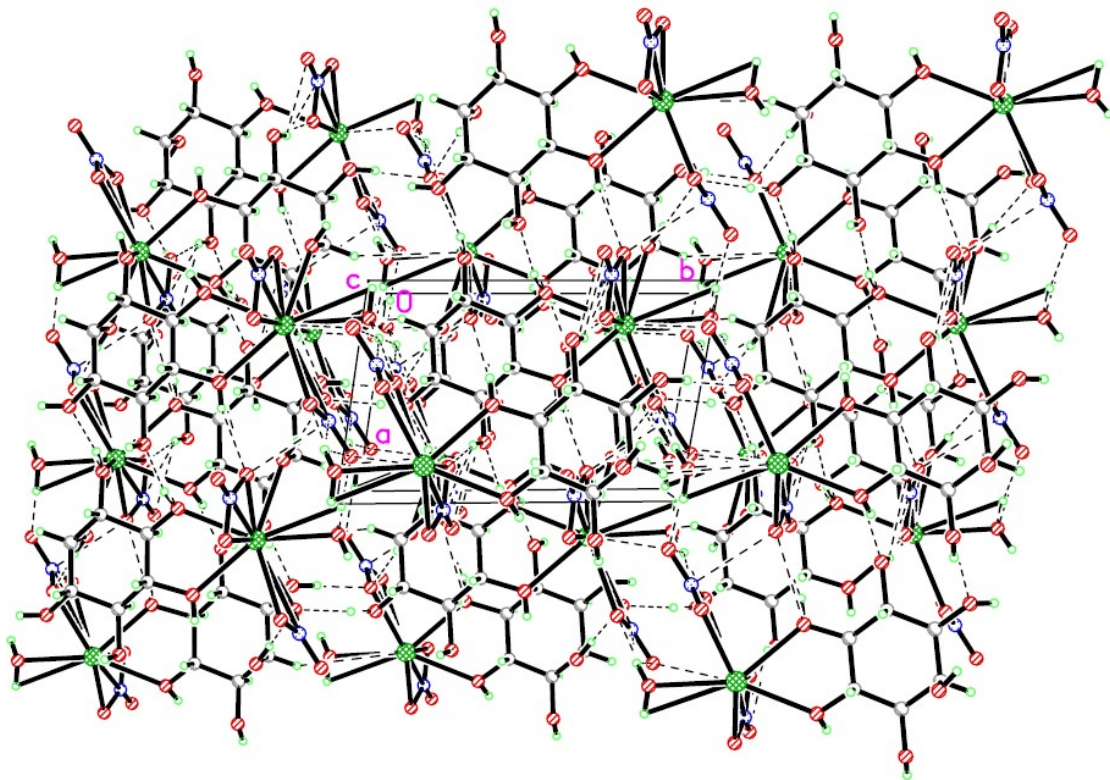


Figure S4-3. The Packing diagram of SrIN along the *c*-axis

Table S4-1. Bond Lengths for SrIN.

	Length/ \AA		Length/ \AA
Sr1–O6	2.5317(15)	O5–C5	1.438(2)
Sr1–O5 ¹	2.5627(15)	O5–Sr1 ¹	2.5627(15)
Sr1–O13	2.5899(17)	O6–C6	1.434(3)
Sr1–O1	2.6157(16)	O7–N1	1.286(2)
Sr1–O10	2.6346(16)	O8–N1	1.260(2)
Sr1–O11	2.6850(16)	O9–N1	1.228(2)
Sr1–O8	2.6855(16)	O10–N2	1.272(2)
Sr1–O4 ¹	2.6998(15)	O11–N2	1.269(2)
Sr1–O7	2.7213(16)	O12–N2	1.224(3)
Sr1–N2	3.087(2)	C1–C6	1.526(3)
Sr1–N1	3.128(2)	C1–C2	1.527(3)
O1–C1	1.426(3)	C2–C3	1.527(3)
O2–C2	1.427(2)	C3–C4	1.531(3)
O3–C3	1.434(3)	C4–C5	1.527(3)
O4–C4	1.434(2)	C5–C6	1.524(3)
O4–Sr1 ¹	2.6997(15)		

¹2-X, 1-Y, 1-Z

Table S4-2. Bond Angles for SrIN.

	Angle/ [°]		Angle/ [°]
O6–Sr1–O5 ¹	86.27(5)	O13–Sr1–N1	69.81(5)
O6–Sr1–O13	152.66(6)	O1–Sr1–N1	73.63(5)
O5 ¹ –Sr1–O13	100.69(5)	O10–Sr1–N1	135.91(5)
O6–Sr1–O1	62.99(5)	O11–Sr1–N1	98.67(5)
O5 ¹ –Sr1–O1	85.90(5)	O8–Sr1–N1	23.47(4)
O13–Sr1–O1	143.25(5)	O4 ¹ –Sr1–N1	132.34(5)
O6–Sr1–O10	72.82(5)	O7–Sr1–N1	24.14(4)
O5 ¹ –Sr1–O10	123.35(5)	N2–Sr1–N1	118.81(5)
O13–Sr1–O10	81.45(5)	C1–O1–Sr1	119.10(13)
O1–Sr1–O10	124.90(5)	C4–O4–Sr1 ¹	120.16(12)
O6–Sr1–O11	78.42(5)	C5–O5–Sr1 ¹	122.42(12)
O5 ¹ –Sr1–O11	164.21(5)	C6–O6–Sr1	117.49(12)
O13–Sr1–O11	91.40(5)	N1–O7–Sr1	95.95(12)
O1–Sr1–O11	90.48(5)	N1–O8–Sr1	98.40(12)
O10–Sr1–O11	48.17(5)	N2–O10–Sr1	98.35(12)
O6–Sr1–O8	128.77(5)	N2–O11–Sr1	96.00(11)
O5 ¹ –Sr1–O8	118.25(5)	O9–N1–O8	121.71(19)
O13–Sr1–O8	70.98(5)	O9–N1–O7	120.73(19)
O1–Sr1–O8	74.09(5)	O8–N1–O7	117.54(18)
O10–Sr1–O8	115.76(5)	O9–N1–Sr1	172.24(15)
O11–Sr1–O8	75.20(5)	O8–N1–Sr1	58.13(11)
O6–Sr1–O4 ¹	85.58(5)	O7–N1–Sr1	59.90(10)
O5 ¹ –Sr1–O4 ¹	60.43(5)	O12–N2–O11	121.73(19)
O13–Sr1–O4 ¹	75.41(5)	O12–N2–O10	120.8(2)
O1–Sr1–O4 ¹	135.84(5)	O11–N2–O10	117.42(18)
O10–Sr1–O4 ¹	65.82(5)	O12–N2–Sr1	177.14(17)
O11–Sr1–O4 ¹	113.95(5)	O11–N2–Sr1	59.87(10)
O8–Sr1–O4 ¹	145.43(5)	O10–N2–Sr1	57.60(10)
O6–Sr1–O7	131.30(5)	O1–C1–C6	105.42(16)
O5 ¹ –Sr1–O7	70.90(5)	O1–C1–C2	111.48(18)
O13–Sr1–O7	75.48(5)	C6–C1–C2	109.78(17)
O1–Sr1–O7	72.71(5)	O2–C2–C1	111.10(17)
O10–Sr1–O7	155.13(5)	O2–C2–C3	112.02(16)
O11–Sr1–O7	122.55(5)	C1–C2–C3	109.79(18)
O8–Sr1–O7	47.49(5)	O3–C3–C2	108.42(17)
O4 ¹ –Sr1–O7	115.89(5)	O3–C3–C4	108.83(17)
O6–Sr1–N2	73.66(5)	C2–C3–C4	111.86(17)
O5 ¹ –Sr1–N2	145.61(5)	O4–C4–C5	106.65(16)
O13–Sr1–N2	86.65(5)	O4–C4–C3	111.43(17)
O1–Sr1–N2	108.17(5)	C5–C4–C3	111.63(17)
O10–Sr1–N2	24.05(5)	O5–C5–C6	108.93(16)
O11–Sr1–N2	24.13(5)	O5–C5–C4	107.81(16)

O8–Sr1–N2	95.97(5)	C6–C5–C4	110.14(17)
O4 ¹ –Sr1–N2	89.87(5)	O6–C6–C5	112.63(17)
O7–Sr1–N2	142.75(5)	O6–C6–C1	109.10(17)
O6–Sr1–N1	136.42(5)	C5–C6–C1	111.54(17)
O5 ¹ –Sr1–N1	95.04(5)		

¹2-X, 1-Y, 1-Z

Table S4-3. Hydrogen Bonds for SrIN.

D–H… A	d(D–H)/Å	d(H…A)/Å	d(D…A)/Å	D–H–A/°
O1–H1… O10 ¹	0.767(16)	2.100(18)	2.840(2)	162(3)
O2– H2… O11 ²	0.82	1.97	2.773(2)	167.0
O3– H3… O7 ³	0.82	1.99	2.801(2)	169.0
O4– H4… O7 ⁴	0.813(16)	2.230(18)	3.012(2)	161(2)
O5– H5… O3 ⁵	0.805(16)	1.889(17)	2.683(2)	168(3)
O6– H6… O2 ⁵	0.791(16)	1.875(17)	2.653(2)	168(3)
O13– H13A… O8 ⁶	0.912(15)	1.995(16)	2.904(2)	174(2)
O13– H13A… O9 ⁶	0.912(15)	2.56(2)	3.115(2)	119.6(18)

¹-1+X, +Y, +Z; ²1-X, 1-Y, -Z; ³+X, 1+Y, +Z; ⁴1-X, 1-Y, 1-Z; ⁵1+X, +Y, +Z; ⁶1-X, -Y, -Z

Table S4-4. Torsion Angles for SrIN.

	Angle/°		Angle/°
Sr1–O8–N1–O9	-170.87(17)	O3–C3–C4–O4	55.2(2)
Sr1–O8–N1–O7	8.00(19)	C2–C3–C4–O4	-64.6(2)
Sr1–O7–N1–O9	171.03(17)	O3–C3–C4–C5	174.33(16)
Sr1–O7–N1–O8	-7.86(19)	C2–C3–C4–C5	54.6(2)
Sr1–O11–N2–O12	-177.2(2)	Sr1 ¹ –O5–C5–C6	-72.70(19)
Sr1–O11–N2–O10	2.45(19)	Sr1 ¹ –O5–C5–C4	46.8(2)
Sr1–O10–N2–O12	177.2(2)	O4–C4–C5–O5	-50.6(2)
Sr1–O10–N2–O11	-2.5(2)	C3–C4–C5–O5	-172.53(16)
Sr1–O1–C1–C6	-39.3(2)	O4–C4–C5–C6	68.1(2)
Sr1–O1–C1–C2	-158.40(12)	C3–C4–C5–C6	-53.8(2)
O1–C1–C2–O2	-60.8(2)	Sr1–O6–C6–C5	-173.49(12)
C6–C1–C2–O2	-177.25(16)	Sr1–O6–C6–C1	-49.07(19)
O1–C1–C2–C3	174.70(16)	O5–C5–C6–O6	-62.0(2)
C6–C1–C2–C3	58.3(2)	C4–C5–C6–O6	179.90(16)
O2–C2–C3–O3	59.7(2)	O5–C5–C6–C1	174.89(17)
C1–C2–C3–O3	-176.40(15)	C4–C5–C6–C1	56.8(2)
O2–C2–C3–C4	179.67(17)	O1–C1–C6–O6	55.2(2)
C1–C2–C3–C4	-56.4(2)	C2–C1–C6–O6	175.43(16)
Sr1 ¹ –O4–C4–C5	37.4(2)	O1–C1–C6–C5	-179.70(17)
Sr1 ¹ –O4–C4–C3	159.44(13)	C2–C1–C6–C5	-59.5(2)

¹2-X, 1-Y, 1-Z

Part 5 The pKa's of *myo*-inositol and galactitol according to the prediction by the chemicalize program

The pKa's of *myo*-inositol according to the prediction by the chemicalize program is shown in Figure S5-1.

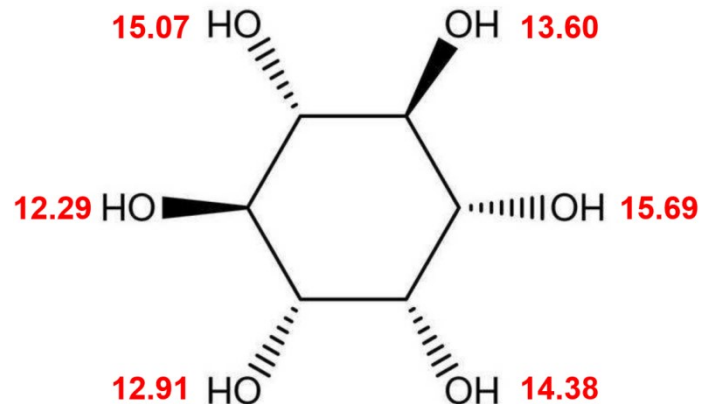


Figure S5-1. The pKa's of *myo*-inositol according to the prediction by the chemicalize program.

Part 6 Mass spectra of LuG, ScI, MnG, and SrIN

The mass spectrum of LuG is shown in Figure S6-1a. A proposed assignment of the six peaks is provided in Table S6-1. According to the assignment, a simulated mass spectrum in the same range was present in Figure S6-1b.

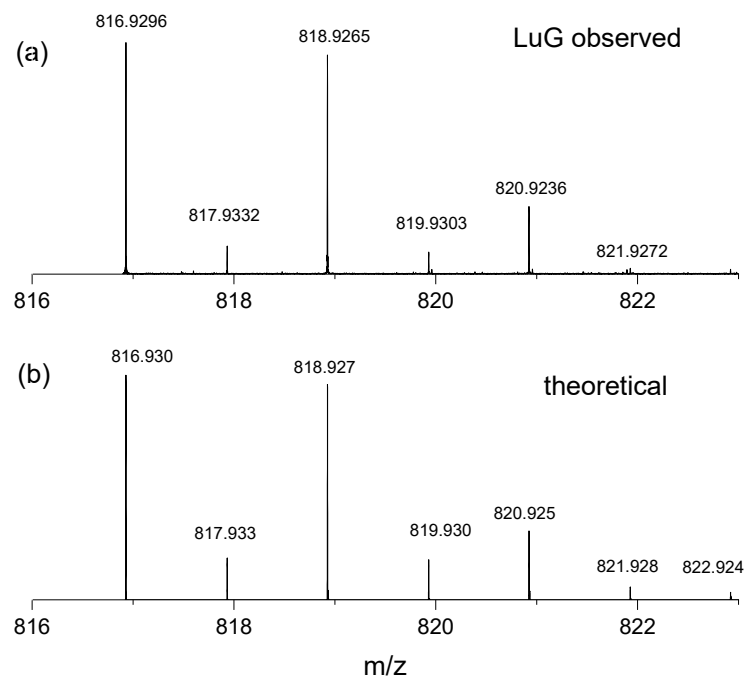


Figure S6-1. Mass spectrum of LuG (a) and a simulated mass spectrum of LuG(b).

Table S6-1. Characterization of the mass spectral peaks in the m/z region of Fig. S6-1

Theoretical m/z	Detected m/z	Elemental composition	The probability of isotope peaks primarily affected by chlorine isotopes
816.929	816.929	$^{12}\text{C}_{12}^{1}\text{H}_{26}^{35}\text{Cl}_3^{175}\text{Lu}_2^{16}\text{O}_{12}$	$C_3^3 \times \frac{3}{4} = \frac{27}{64}$
817.933	817.933	$^{12}\text{C}_{11}^{13}\text{C}_1^{16}\text{O}_{12}^{175}\text{Lu}_2^{1}\text{H}_{26}^{35}\text{Cl}_3$	
818.927	818.926	$^{12}\text{C}_{12}^{1}\text{H}_{26}^{35}\text{Cl}_2^{37}\text{Cl}_1^{175}\text{Lu}_2^{16}\text{O}_{12}$	$C_3^1 \times \frac{3}{4} \times \frac{1}{4} = \frac{27}{64}$
819.930	819.930	$^{12}\text{C}_{11}^{13}\text{C}_1^{16}\text{O}_{12}^{175}\text{Lu}_2^{1}\text{H}_{26}^{35}\text{Cl}_2^{37}\text{Cl}_1$	
820.925	820.923	$^{12}\text{C}_{12}^{16}\text{O}_{12}^{175}\text{Lu}_2^{1}\text{H}_{26}^{35}\text{Cl}_1^{37}\text{Cl}_2$	$C_3^2 \times \frac{3}{4} \times \frac{1}{4} = \frac{9}{64}$
821.927	821.927	$^{12}\text{C}_{11}^{13}\text{C}_1^{16}\text{O}_{12}^{175}\text{Lu}_2^{1}\text{H}_{26}^{35}\text{Cl}_1^{37}\text{Cl}_2$	

The mass spectrum of ScI is shown in Figure S6-2a. A proposed assignment of the six peaks is provided in Table S6-2. According to the assignment, a simulated mass spectrum in the same range was present in Figure S6-2b.

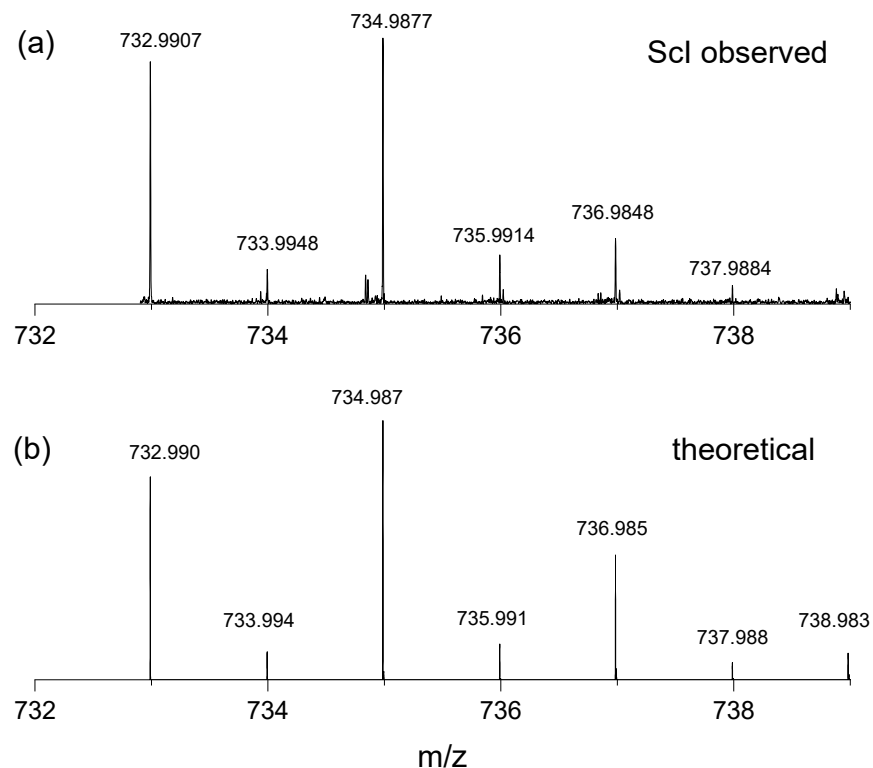


Figure S6-2. Mass spectrum of ScI sample (a) experimental (b) theoretical.

Table S6-2. Characterization of the mass spectral peaks in the m/z region of Fig. S6-2

Theoretical m/z	Detected m/z	Elemental composition	The probability of isotope peaks primarily affected by chlorine isotopes
732.990	732.990	$^{12}\text{C}_{12}^{1}\text{H}_{39}^{35}\text{Cl}_4^{16}\text{O}_{20}^{45}\text{Sc}_2$	$C_4^4 \times \frac{3}{4} = \frac{81}{256}$
733.993	733.994	$^{12}\text{C}_{11}^{13}\text{C}_1^{16}\text{O}_{20}^{1}\text{H}_{39}^{35}\text{Cl}_4^{45}\text{Sc}_2$	
734.987	734.987	$^{12}\text{C}_{12}^{1}\text{H}_{39}^{35}\text{Cl}_3^{37}\text{Cl}_1^{16}\text{O}_{20}^{45}\text{Sc}_2$	$C_4^1 \times \frac{3}{4} \times \frac{1}{4} = \frac{108}{256}$
735.990	735.991	$^{12}\text{C}_{11}^{13}\text{C}_1^{16}\text{O}_{20}^{1}\text{H}_{39}^{35}\text{Cl}_3^{37}\text{Cl}_1^{45}\text{Sc}_2$	
736.985	736.984	$^{12}\text{C}_{12}^{16}\text{O}_{20}^{1}\text{H}_{39}^{35}\text{Cl}_2^{37}\text{Cl}_2^{45}\text{Sc}_2$	$C_4^2 \times \frac{3}{4} \times \frac{1}{4} = \frac{54}{256}$
737.988	737.988	$^{12}\text{C}_{11}^{13}\text{C}_1^{16}\text{O}_{20}^{1}\text{H}_{39}^{35}\text{Cl}_2^{37}\text{Cl}_2^{45}\text{Sc}_2$	

The mass spectrum of MnG is shown in **Figure S6-3**. Only two types of fragment peaks are observed: 1) the fragment contains one positive charge; 2) the fragment contains 2 positive charges.

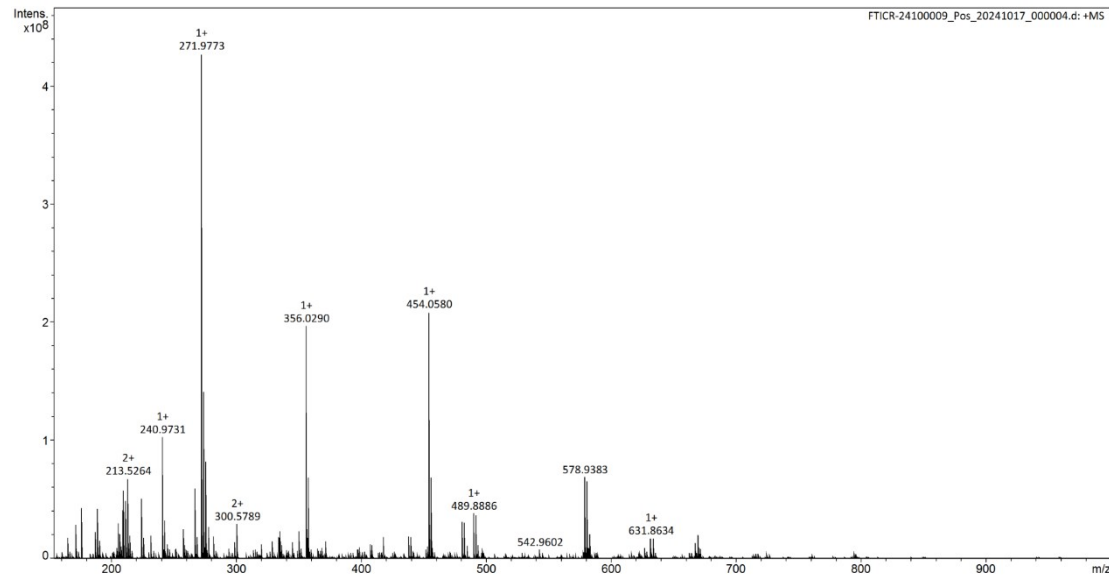


Figure S6-3. A MS spectrum of the $\text{MnCl}_2/\text{galactitol}$ system

Firstly, we consider the fragment peak with one positive charge. We compare the m/z of each peak in the MS spectrum shown in **Figure S6-3** with the m/z value of each of the possible fragments of the proposed complexes where deprotonation occurs on alditol ligands. We found the minimal difference between the m/z value of the observed peaks and those of the possible fragments are larger than 0.01. It should be pointed out that the MS spectrum shown in **Figure S6-3** is a high-resolution spectrum. When the differences in the m/z between the observed peak and the proposed fragment are larger than 0.001, the proposed fragment cannot be assigned to the observed peak. Therefore, we can say the possible fragments with +1 charge from the proposed complexes where deprotonation occurs on the alditol moiety are not present in the MS spectrum in **Figure S6-3**.

Then, we come to the peaks in the MS spectrum where the corresponding fragment possesses 2 positive charges. We compare the m/z of each peak in the MS spectrum

shown in **Figure S6-3** with the m/z value of each of the possible fragments. We found the minimal difference between the m/z value of the observed peaks and those of the possible fragments is larger than 0.68. Therefore, we can say that the possible fragments with +2 charge from the proposed complexes where deprotonation occurs on the alditol moiety are not present in the MS spectrum in **Figure S6-3**.

In summary, no fragment containing deprotonated galactitol is found in the MS spectrum shown in **Figure S6-3**.

The mass spectrum of SrIN is shown in **Figure S6-4**. Only two types of fragment peaks are observed: 1) the fragment contains one positive charge; 2) the fragment contains two positive charges.

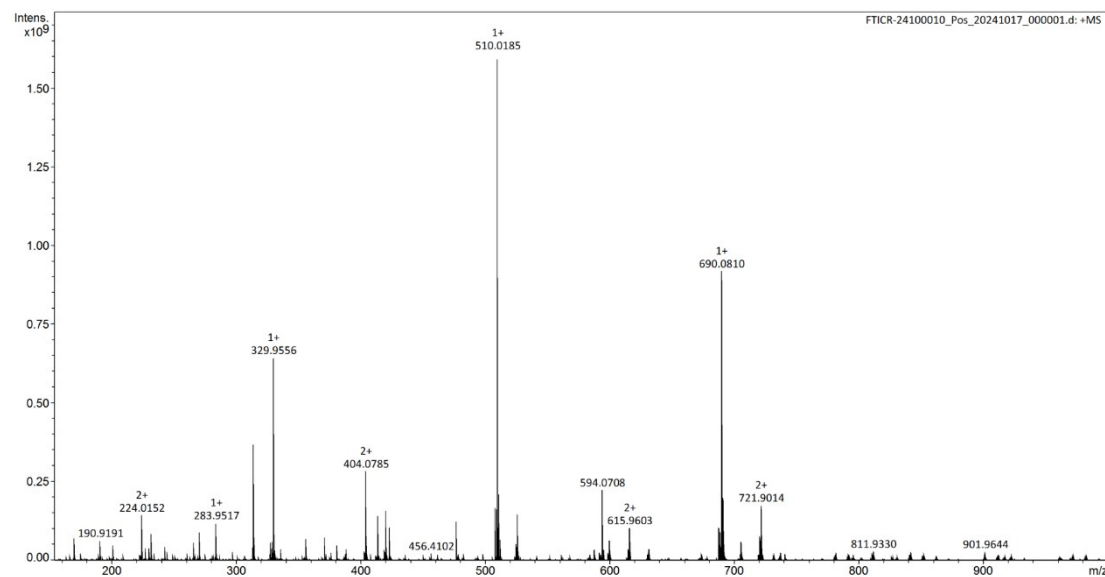


Figure S6-4 A MS spectrum of the $\text{Sr}(\text{NO}_3)_2/\text{myo}$ -inositol system

Firstly, we consider the fragment peak with one positive charge. We compare the m/z of each peak in the MS spectrum shown in **Figure S6-4** with the m/z value of each of the possible fragments of the proposed complexes where deprotonation occurs on the alditol moiety. We found the minimal difference between the m/z value of the observed peaks and those of the possible fragments are larger than 0.01. It should be pointed out

that the MS spectrum shown in **Figure S6-4** is a high-resolution spectrum. When the differences in the m/z between the observed peak and the proposed fragment are larger than 0.001, the proposed fragment cannot be assigned to the observed peak. Therefore, we can say the possible fragments with +1 charge from the proposed complexes where deprotonation occurs on alditol moiety are not present in the MS spectrum in **Figure S6-4**.

Then, we come to the peaks in the MS spectrum where the corresponding fragment possesses two positive charges. We compare the m/z of each peak in the MS spectrum shown in **Figure S6-4** with the m/z value of each of the possible fragments of the proposed complexes where deprotonation occurs on alditol moiety. We found the minimal difference between the m/z value of the observed peaks and those of the possible fragments are larger than 0.01. Therefore, we can say that the possible fragments with +2 charge from the proposed complexes where deprotonation occurs on the alditol moiety are not present in the MS spectrum in **Figure S6-4**.

In summary, no fragment containing deprotonated *myo*-inositol is found in the MS spectrum shown in **Figure S6-4**.

Therefore, we cannot find any characteristic peak of the complex containing deprotonated alditol either $\text{Sr}(\text{NO}_3)_2/\text{myo}$ -inositol system or $\text{MnCl}_2/\text{galactitol}$ system from the corresponding MS spectra shown in **Figure S6-3** and **Figure S6-4**, respectively.

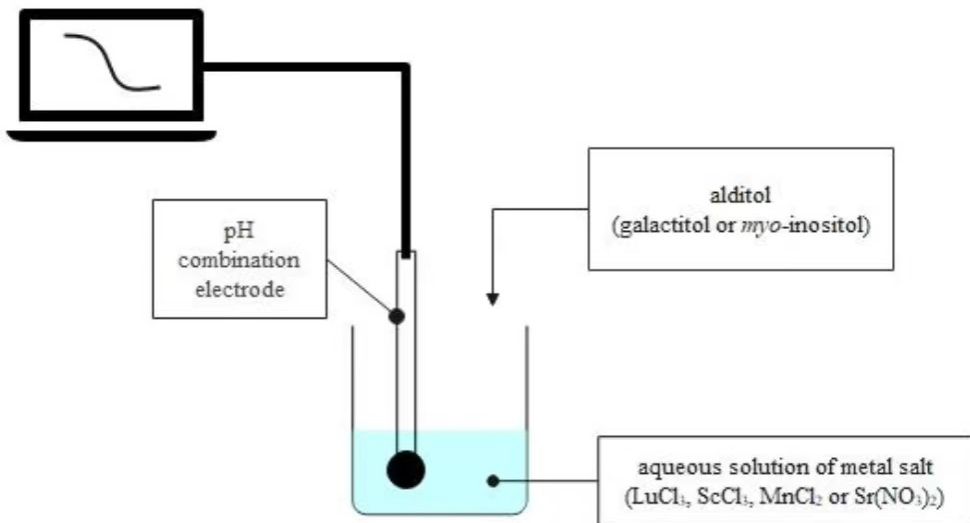
Part 7 The Variation of pH Values of Aqueous Solutions upon Addition of Alditols

Experimental Procedures

Aqueous solutions of LuCl₃·6H₂O, ScCl₃·6H₂O, MnCl₂·4H₂O, and Sr(NO₃)₂ were prepared. The initial concentrations of the metal salts in the four solutions are listed in Table S7-1. The volumes of each of the four solutions were 100 ml. To prevent the evaporation of the solvent, the beaker containing the solution was covered by a plastic film. Upon preparation, the solutions were kept stirring, meanwhile, the pH values of the solutions were monitored as a function of time. The pH values of the solution were automatically measured and collected on a desktop (Scheme S7-1). After the solutions reached equilibrium states, 0.016 mol of alditol was added to each solution, and the variation in the pH value was recorded.

Table S7-1. The initial concentrations of the metal salts and alditol

	Metal ion (mol/L)	Ligand (mol/L)
LuG	0.30	0.16
ScI	0.30	0.16
MnG	0.30	0.16
SrIN	0.30	0.16



Scheme S7-1. Schematic diagram of the pH experimental setup to monitor the pH variation of the four systems (Lu^{3+} /galactitol, Sc^{3+} /*myo*-inositol, Mn^{2+} /galactitol, and Sr^{2+} /*myo*-inositol)

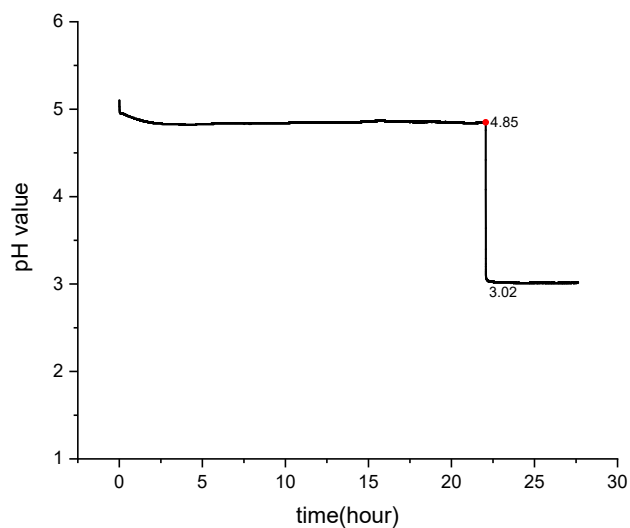


Figure S7-1. The variation of the pH values as a function of time in the Lu^{3+} /galactitol system (The event that galactitol powder was added into the solution was labeled by a red point).

The experimental results on the $\text{Sc}^{3+}/\text{myo}$ -inositol system.

In the experiment, 7.78 g $\text{ScCl}_3 \cdot 6\text{H}_2\text{O}$ was dissolved in water so that 100 ml aqueous solution of Sc^{3+} was prepared and the initial concentration of Sc^{3+} was 0.30 mol/L. The initial pH value of the solution was 2.79, which indicates that obvious hydrolysis of Sc^{3+} occurs. During the first five hours, the pH value of the solution decreased gradually from 2.79 to 2.68. The variation in the pH value of the solution can be attributed to the additional slow hydrolysis of Sc^{3+} in the aqueous solution. Subsequently, the solution was further stirred for about 20 hours, during this period, no significant variation on the pH value of the solution can be found. Thus, the solution can be regarded as reaching an equilibrium state and no further hydrolysis of Sc^{3+} takes place. Then, 2.88 g (16 mmol) *myo*-inositol powder was added to the solution. As *myo*-inositol was introduced into the solution, an abrupt dive of the pH value (from 2.68 to 1.71) of the solution within one minute was observed (Figure S7-2). The significant reduction in the pH value of the solution implies that a large amount of free protons are released into the solution. The amount of free proton released can be calculated as: $100 \times 10^{-3} \times (10^{-1.71} - 10^{-2.68}) = 1.74 \times 10^{-3}$ mol. Because of the same reason as that in the $\text{Lu}^{3+}/\text{galactitol}$ system, the released free proton should come from *myo*-inositol molecules. That is to say, 10.9% ($1.74 \times 10^{-3} / 0.016$) of *myo*-inositol molecules took part in the deprotonation. The higher percentage of *myo*-inositol involved in the deprotonation reaction may be related to the fact the ionic radius of Sc^{3+} (0.0870nm, CN=8) is significantly smaller than that of Lu^{3+} (0.0977nm, CN=8).

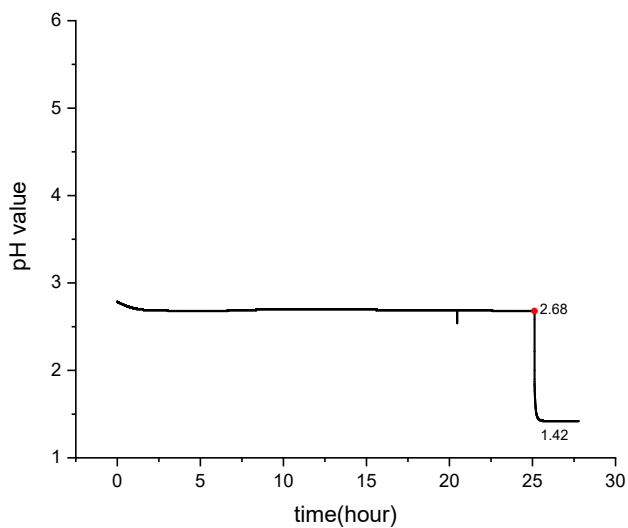


Figure S7-2. The variation of the pH values as a function of time in the $\text{Sc}^{3+}/\text{myo}$ -inositol system (The event that *myo*-inositol powder was added into the solution was labeled by a red point).

The experimental results on the Mn^{2+} /galactitol system.

In the experiment, water was first boiled to remove dissolved oxygen in the water. Then, the water was allowed to cool down to room temperature. Afterward, 5.93 g (0.030 mol) $\text{MnCl}_2 \cdot 4\text{H}_2\text{O}$ was dissolved in the de-oxygenated water. Thus, 100 ml of aqueous solution of Mn^{2+} was prepared and the initial concentration of Mn^{2+} was 0.30 mol/L. Upon preparation, the solution was kept stirring, meanwhile, the pH value of the solution was monitored as a function of time. The initial pH value of the solution was 4.95, which implies slight hydrolysis of Mn^{2+} took place as Mn^{2+} is dissolved in the solution. During the first five hours, the pH value of the solution increased gradually from 4.95 to 5.04. Subsequently, the solution was further stirred for about 19 hours, during this period, no significant variation on the pH value of the solution can be found. Thus, the solution can be regarded as reaching an equilibrium state. Then, 3.00 g (16

mmol) galactitol powder was added to the solution. As galactitol was introduced into the solution, a slight drop in the pH value (from 4.97 to 4.80) of the solution was observed (Figure S7-3). Since the variation of the pH value is small (about 0.2), an insignificant amount of free proton was released. The amount of free protons is calculated to be $100 \times 10^{-3} \times (10^{-4.80} - 10^{-4.97}) = 5.13 \times 10^{-7}$ mol. If the released free proton is from galactitol, the percentage of deprotonation on galactitol in the Mn^{2+} /galactitol system is calculated to be 0.003% ($5.13 \times 10^{-7} / 0.016$). Thus, Mn^{2+} cannot bring about remarkable deprotonation on galactitol molecules.

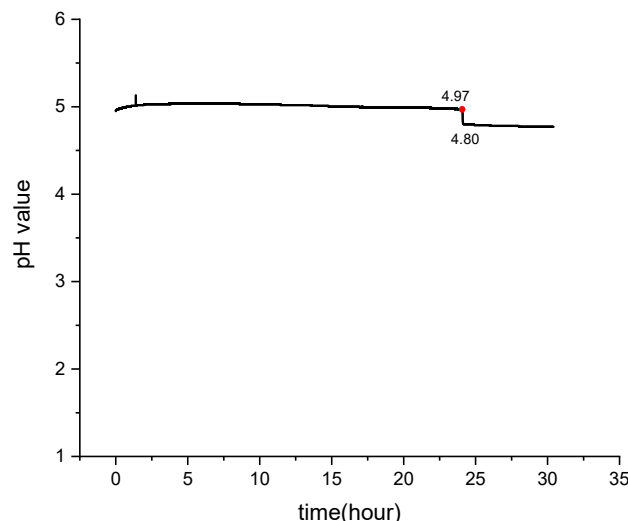


Figure S7-3 The variation of the pH values as a function of time in the Mn^{2+} /galactitol system (The event that galactitol powder was added into the solution was labeled by a red point).

The experimental results on $\text{Sr}^{2+}/\text{myo}$ -inositol system.

In the experiment, 6.34 g (0.030 mol) $\text{Sr}(\text{NO}_3)_2$ was dissolved in water so that 100 ml aqueous solution of Sr^{2+} was prepared, and the initial concentration of Sr^{2+} was 0.30 mol/L. Upon preparation, the solution was kept stirring, meanwhile, the pH value of the solution was monitored as a function of time. The initial pH value of the solution was

4.98, which implies slight hydrolysis of Sr^{2+} takes place as Sr^{2+} was dissolved in the solution. During the first five hours, the pH value of the solution increased gradually from 4.98 to 5.11. Subsequently, the solution was further stirred for about 19 hours, during this period, no significant variation on the pH value of the solution can be found. Thus, the solution can be regarded as reaching an equilibrium state. Then, 2.88 g (16 mmol) *myo*-inositol powder was added to the solution. As *myo*-inositol was introduced into the solution, a slight drop in the pH value (from 5.08 to 4.83) of the solution was observed (Figure S7-4). Since the variation of the pH value is small (about 0.2), an insignificant amount of free proton was released. The amount of free protons is calculated to be $100 \times 10^{-3} \times (10^{-4.83} - 10^{-5.08}) = 6.47 \times 10^{-7}$ mol. If the released free proton is from *myo*-inositol, The percentage of deprotonation on *myo*-inositol in the $\text{Sr}^{2+}/\text{myo}$ -inositol system is calculated to be 0.004% ($6.47 \times 10^{-7} / 0.016$). Thus, Sr^{2+} cannot bring about remarkable deprotonation on *myo*-inositol molecules.

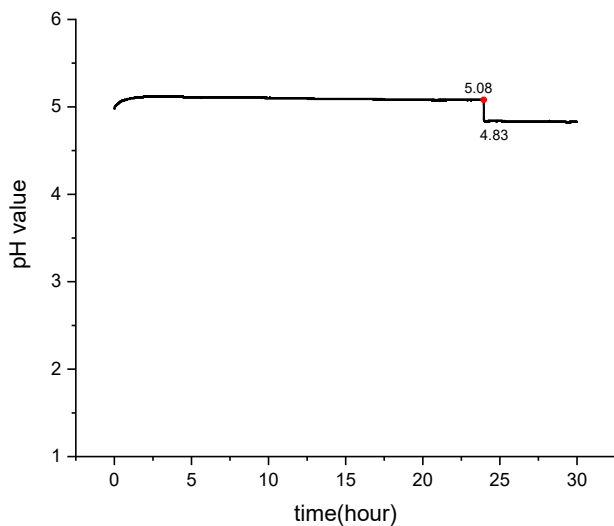


Figure S7-4. The variation of the pH values as a function of time in the $\text{Sr}^{2+}/\text{myo}$ -inositol system (The event that *myo*-inositol powder was added into the solution was labeled by a red point).

Part 8 The bond lengths of coordination bonds and torsion angles in ScI and ErI

Table S8-1. The bond lengths of coordination bonds in ScI and ErI

ScI		ErI			
	Length/Å		Length/Å	Length/Å	
Sc1–O1	2.0686(14)	Er1–O1	2.2202(11)	Er2–O1 ¹	2.2572(11)
Sc1–O1 ¹	2.0894(13)	Er1–O1 ¹	2.2202(11)	Er2–O1	2.2572(11)
Sc1–O8	2.1631(16)	Er1–O7	2.291(2)	Er2–O9 ¹	2.3493(13)
Sc1–O7	2.1915(15)	Er1–O2 ¹	2.3693(13)	Er2–O9	2.3493(13)
Sc1–O6 ¹	2.2410(15)	Er1–O2	2.3693(13)	Er2–O6	2.3759(12)
Sc1–O2	2.2628(15)	Er1–Cl1 ¹	2.6437(5)	Er2–O6 ¹	2.3759(12)
Sc1–Cl1	2.4679(7)	Er1–Cl1	2.6437(5)	Er2–O8 ¹	2.3856(13)
				Er2–O8	2.3857(13)

ScI: ¹1-X, 1-Y, 1-Z; ErI: ¹1-X, +Y, 1/2-Z

Table S8-2 Torsion Angles for ScI and ErI.

ScI		ErI	
	Angle/ ^o		Angle/ ^o
O1–C1–C2–O2	-39.9(2)	O1–C1–C2–O2	42.23(18)
C6–C1–C2–O2	-158.61(15)	C6–C1–C2–O2	163.44(14)
O1–C1–C2–C3	80.0(2)	O1–C1–C2–C3	-76.67(18)
C6–C1–C2–C3	-38.8(2)	C6–C1–C2–C3	44.5(2)
O2–C2–C3–O3	-72.13(19)	O2–C2–C3–O3	68.59(17)
C1–C2–C3–O3	170.21(16)	C1–C2–C3–O3	-173.37(14)
O2–C2–C3–C4	168.08(15)	O2–C2–C3–C4	-171.60(14)
C1–C2–C3–C4	50.4(2)	C1–C2–C3–C4	-53.56(19)
O3–C3–C4–O4	59.0(2)	O3–C3–C4–O4	-57.66(18)
C2–C3–C4–O4	179.25(15)	C2–C3–C4–O4	-177.64(14)
O3–C3–C4–C5	176.92(16)	O3–C3–C4–C5	-178.02(13)
C2–C3–C4–C5	-62.8(2)	C2–C3–C4–C5	62.0(2)
O4–C4–C5–O5	-53.8(2)	O4–C4–C5–O5	59.91(19)
C3–C4–C5–O5	-175.14(16)	C3–C4–C5–O5	177.97(13)
O4–C4–C5–C6	-174.59(16)	O4–C4–C5–C6	-179.82(15)
C3–C4–C5–C6	64.1(2)	C3–C4–C5–C6	-61.8(2)
O5–C5–C6–O6	68.5(2)	O5–C5–C6–O6	-69.74(17)
C4–C5–C6–O6	-171.47(16)	C4–C5–C6–O6	170.89(14)
O5–C5–C6–C1	-173.75(15)	O5–C5–C6–C1	172.12(14)
C4–C5–C6–C1	-53.7(2)	C4–C5–C6–C1	52.74(19)
O1–C1–C6–O6	41.03(19)	O1–C1–C6–O6	-42.10(18)
C2–C1–C6–O6	160.09(16)	C2–C1–C6–O6	-163.20(14)
O1–C1–C6–C5	-78.32(19)	O1–C1–C6–C5	77.01(18)
C2–C1–C6–C5	40.7(2)	C2–C1–C6–C5	-44.1(2)

ScI: ¹1-X, 1-Y, 1-Z

Part 9 The structural characteristics of galactitol and its metal complexes

Table S9-1. The C–C–C–C torsion angles, O1…O4 and C1…C4 distances, $\angle\text{OMO}$ (oxygen atoms only from coordinated OH of galactitol) in the structures of galactitol and its metal complexes

CCDC No.	substance	C1–C2–C3–C4/ ^o	C2–C3–C4–C5/ ^o	C3–C4–C5–C6/ ^o	O1…O4	O6…O3	C1…C4	C6…C3	$\angle\text{OMO}$ (oxygen atoms only from coordinated OH of galactitol)	Ref.	Abbr.
1163340	C ₆ H ₁₄ O ₆	-175.17	170.71	172.56	5.056	5.120	3.889	3.866	57.81	S1	G
192440	CaCl ₂ ·C ₆ H ₁₄ O ₆ ·4H ₂ O	-163.74	-176.32	162.83	5.147	4.995	3.870	3.865	64.12	S2	CaG
192441	2EuCl ₃ ·C ₆ H ₁₄ O ₆ ·14H ₂ O	-174.37	180	174.37	5.220	5.220	3.905	3.905	62.99	63.68	69.44
268325	2LaCl ₃ ·C ₆ H ₁₄ O ₆ ·10H ₂ O	-176.49	-180	176.49	5.225	5.225	3.905	3.905	60.61	62.11	67.34
268326	SrCl ₂ ·C ₆ H ₁₄ O ₆	-171.24	-180	171.24	5.233	5.233	3.914	3.914	63.41	63.80	67.58
658398	La(NO ₃) ₃ ·C ₆ H ₁₄ O ₆ ·4H ₂ O	-156.55	-175.15	163.48	5.150	5.091	3.870	3.866	56.78	58.38	60.86
									62.44	66.91	69.66
658399	2Ca(NO ₃) ₂ ·C ₆ H ₁₄ O ₆ ·H ₂ O	-170.79	-180	170.79	4.429	4.429	3.897	3.897	64.36	S4	CaGN
658400	Sr(NO ₃) ₂ ·C ₆ H ₁₄ O ₆	171.46	-180	-171.46	4.446	4.446	3.896	3.896	59.50	S4	SrGN
790722	2GdCl ₃ ·C ₆ H ₁₄ O ₆ ·14H ₂ O	-174.72	-180	174.72	5.226	5.226	3.908	3.908	63.41	63.90	69.99
794376	Tb(NO ₃) ₃ ·C ₆ H ₁₄ O ₆	170.10	180	-170.10	5.146	5.146	3.883	3.883	66.10	66.32	69.22
		173.27	-180	-173.27	5.073	5.073	3.873	3.873	65.77	66.18	67.91
794377	Sm(NO ₃) ₃ ·C ₆ H ₁₄ O ₆	171.05	-180	-171.05	5.157	5.157	3.887	3.887	65.36	65.50	68.31
		173.51	180	-173.51	5.087	5.087	3.887	3.887	64.82	65.54	67.73
794378	Tb(NO ₃) ₃ ·C ₆ H ₁₄ O ₆ ·3H ₂ O	-169.15	-180	169.15	5.150	5.150	3.878	3.878	64.18	65.81	69.43
		172.21	-180	-172.21	5.198	5.198	3.915	3.915	64.59	64.84	70.69
1102107	SrCl ₂ ·C ₆ H ₁₄ O ₆ ·4H ₂ O	167.00	180	-167.00	5.108	5.108	3.868	3.868	61.90	S7	SrGI
1119394	2SmCl ₃ ·C ₆ H ₁₄ O ₆ ·14H ₂ O	-174.09	-180	174.09	5.217	5.217	3.896	3.896	62.92	63.65	69.28
1149283	2TbCl ₃ ·C ₆ H ₁₄ O ₆ ·14H ₂ O	-173.62	180	173.62	5.223	5.223	3.899	3.899	63.39	63.92	69.93
1170991	LaCl ₃ ·C ₆ H ₁₄ O ₆ ·6H ₂ O	166.50	180	-166.50	5.221	5.221	3.901	3.901	58.67	61.41	67.56
		-171.04	-180	171.04	5.240	5.240	3.904	3.904	59.01	60.19	68.92
1297516	2NdCl ₃ ·C ₆ H ₁₄ O ₆ ·14H ₂ O	174.02	-180	-174.02	5.227	5.227	3.910	3.910	62.47	63.37	68.76
									S11	NdG	

1469993	$2\text{MnCl}_2 \cdot \text{C}_6\text{H}_{14}\text{O}_6 \cdot 2\text{H}_2\text{O}$	159.80	180	-159.80	5.047	5.047	3.870	3.870	72.23		MnG	
2211187	$2\text{LuCl}_2 \cdot 2\text{C}_6\text{H}_{13}\text{O}_6 \cdot 4\text{H}_2\text{O}$	-47.8	177.6	-170.3	2.830	5.146	3.004	3.900	67.57	68.77	69.38	LuG
									73.96	75.90	76.38	
1174959	$\text{Li}_2[\text{Cu}(\text{C}_6\text{H}_{10}\text{O}_6)] \cdot 10\text{H}_2\text{O}^{\text{a}}$	-58.24	-180	58.24	2.482	2.482	3.296	3.296	84.53		S12	LiCuG
	$2\text{PrCl}_3 \cdot \text{C}_6\text{H}_{14}\text{O}_6 \cdot 14\text{H}_2\text{O}^{\text{b}}$										S13	
	$2\text{Nd}(\text{NO}_3)_3 \cdot \text{C}_6\text{H}_{14}\text{O}_6 \cdot 8\text{ H}_2\text{O}^{\text{b}}$										S14	
	$\text{Nd}(\text{NO}_3)_3 \cdot \text{C}_6\text{H}_{14}\text{O}_6^{\text{b}}$											

^a four OHs of galactitol are deprotonated; ^b They can not be found in the CCDC database.

The related references in Table S9-1 are as follows:

- S1 H. M. Berman, R. D. Rosenstein, *Acta Crystallogr. Sect. B: Struct. Crystallogr. Cryst. Chem.* **1968**, *24*, 435–441.
- S2 L. M. Yang, Y. L. Su, W. Liu, X. L. Jin, J. G. Wu, *Carbohydr. Res.* **2002**, *337*, 1485–1493.
- S3 Y. L. Su, L. M. Yang, Z. M. Wang, X. L. Jin, S. F. Weng, C. H. Yan, Z. W. Yu, J. G. Wu, *Carbohydr. Res.* **2006**, *341*, 75–83.
- S4 Y. L. Su, L. M. Yang, Y. Z. Xu, Z. M. Wang, S. F. Weng, C. H. Yan, D. J. Wang, J. G. Wu, *Inorg. Chem.* **2007**, *46*, 5508–5517.
- S5 L. Yu, X. H. Hua, Y. J. Zhai, L. M. Yang, G. Z. Zhao, T. H. Meng, S. F. Weng, Y. Z. Xu, K. X. Liu, J. G. Wu, J. E. Chen, *Chem. J. Chin. Univ.* **2011**, *32*, 1244–1249.
- S6 L. Yu, X. H. Hua, Q. H. Pan, L. M. Yang, Y. Z. Xu, G. Z. Zhao, H. Wang, H. Y. Wang, J. G. Wu, K. X. Liu, J. E. Chen, *Carbohydr. Res.* **2011**, *346*, 2278–2284.
- S7 Y. L. Su, L. M. Yang, Z. M. Wang, S. F. Weng, C. H. Yan, J. G. Wu, *J. Inorg. Biochem.* **2003**, *94*, 43–49.
- S8 L. M. Yang, W. Tian, Y. Zhao, X. L. Jin, S. F. Weng, J. G. Wu, G. X. Xu, *J. Inorg. Biochem.* **2001**, *83*, 161–167.
- S9 L. M. Yang, Y. Zhao, Y. L. Su, Z. M. Wang, C. H. Yan, J. G. Wu, *Chem. J. Chin. Univ.* **2002**, *23*, 1475–1479.
- S10 Y. L. Su, L. M. Yang, X. L. Jin, S. F. Weng, J. G. Wu, *J. Mol. Struct. (Mol. Phys.)* **2002**, *616*, 221–230.
- S11 L. M. Yang, Y. Zhao, W. Tian, X. L. Jin, S. F. Weng, J. G. Wu, *Carbohydr. Res.* **2001**, *330*, 125–130.
- S12 P. Klufers, J. Schuhmacher, *Angew. Chem. Inter. Ed.* **1994**, *33*, 1742–1744.

S13 S. J. Angyal, D. C. Craig, *Carbohydr. Res.* **1993**, *241*, 1–8.

S14 Y. L. Su, L. M. Yang, Z. M. Wang, C. H. Yan, S. F. Weng and J. G. Wu, *Carbohydr. Res.* **2003**, *338*, 2029–2034.

Part 10 Quantum chemistry calculation results for galactitol

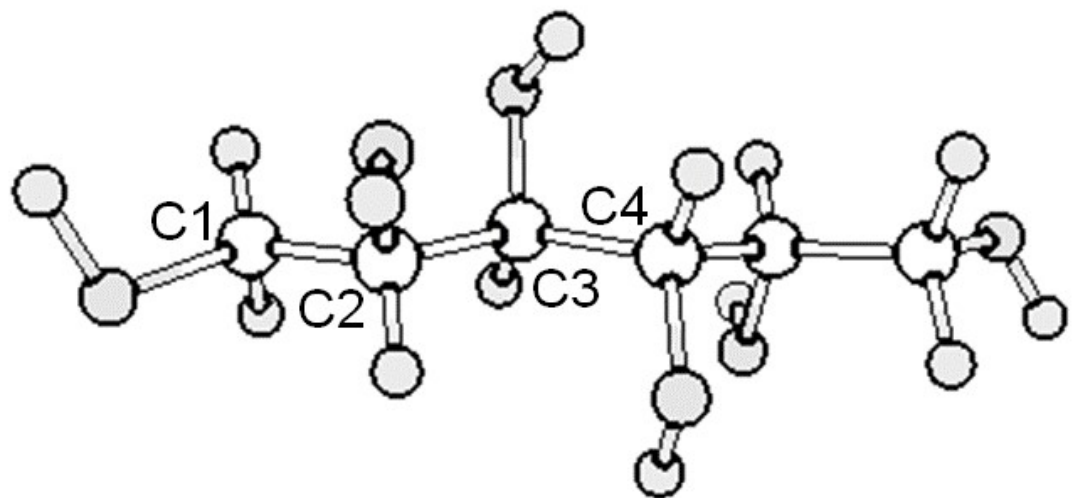


Figure S10-1. The torsion angle of C1–C2–C3–C4 in galactitol

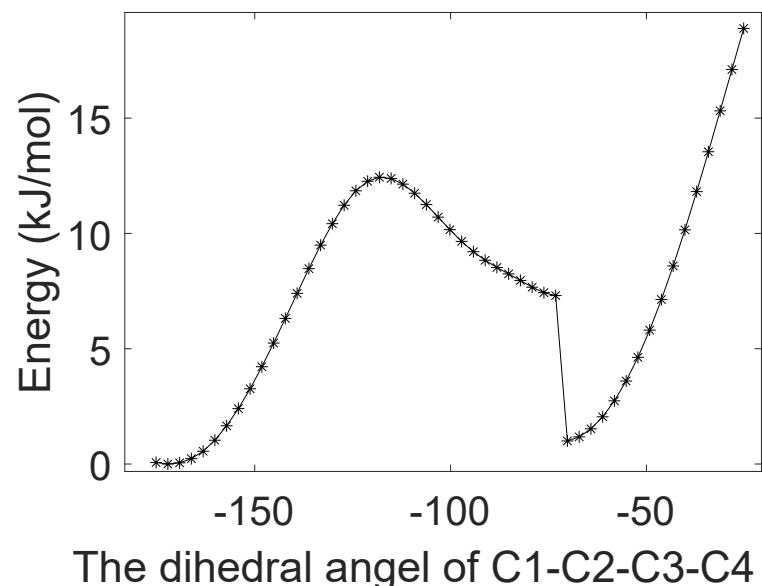


Figure S10-2. The relationship between the steric energy of the galactitol molecule and the dihedral angle of C1–C2–C3–C4

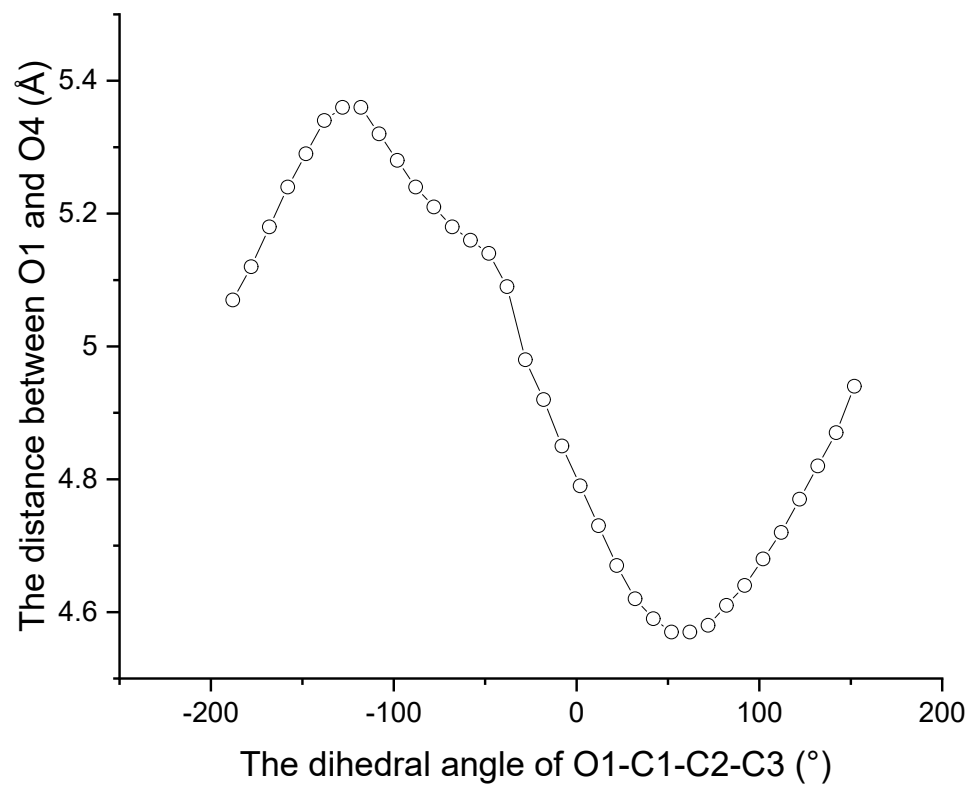


Figure S10-3. The relationship between the O1…O4 distance of the galactitol molecule and the dihedral angle of O1–C1–C2–C3